# Cluster Framework Structures and Relationships. Two Compounds with a New Connectivity, $K_2Zr_6Cl_{15}B$ and $K_3Zr_6Cl_{15}Be$

**Robin P. Ziebarth and John D. Corbett***

*Contribution from the Department of Chemistry, Iowa State University, Ames, Iowa 50011.*
*Received May 11, 1987*

**Abstract:** The title compounds are obtained in high yield by reaction of stoichiometric quantities of $ZrCl_4$, KCl, powdered Zr, and the interstitial element B or Be in sealed tantalum containers at 800–850 °C for 2–3 weeks. The structures were established by single-crystal means to be orthorhombic for $K_2Zr_6Cl_{15}B$ (*Cccm*, $Z = 4$, $R = 3.3$, $R_w = 4.1$) and monoclinic for $K_3Zr_6Cl_{15}Be$ (*C*2/*c*, $Z = 4$, $R = 4.8$, $R_w = 3.2$). Both contain crisscrossing linear chains of trans-bridged clusters $\cdots[Zr_6Cl_{12}B(Be)]-Cl^{a-a}\cdots$ that are further interconnected by bent $Cl^{a-a}$ bridges at the remaining four metal vertices. The low symmetry of one cation site in $K_2Zr_6Cl_{15}B$ is noteworthy. The change of the interstitial atom in $K_3Zr_6Cl_{15}Be$ forces an orthorhombic to monoclinic structural distortion in order to accommodate a third cation. The distortion is accomplished mainly by rotation of the linear chains in alternate directions, which splits the former low-symmetry cation site into two. The four distinct $(M_6X_{12})X^{a-a}_{6/2}$ framework structures exhibited in the $Ta_6Cl_{15}$, $CsNb_6Cl_{15}$, $K_2Zr_6Cl_{15}B$, and $Nb_6F_{15}$ parent types are compared and systematized in terms of the three-dimensional cluster connectivity, ring size, and local $Cl^{a-a}$ geometry. The choice among these for various $M^1_x(Zr_6Cl_{12}Z)Cl_{6/2}$ compounds is evidently dictated by the size of the interstitial Z and the need to accommodate cations of various sizes and numbers, and the last is in turn largely governed by the electronic nature of the interstitial element Z.

Zirconium halide clusters have recently been found to provide an unprecedented diversity of phases and structures because of several especially novel features. All of these compounds utilize the $Zr_6X_{12}$ building block, that is, a cluster in which halide (X) bridges all edges of a nominal metal octahedron. The most significant feature of these clusters is that an interstitial atom Z is present within all known examples, this atom contributing both valence electrons and strong Zr–Z bonding.[1-6] The most favorable electron count therein is in the neighborhood of 14 when Z is a representative element, so that alteration in the electronic nature of Z allows the formation of a series of phases of stoichiometries $(Zr_6X_{12}Z)X_n$, $0 \le n \le 6$. In this way the phases $Zr_6Cl_{12}Be$, $Zr_6Cl_{13}B$, $Zr_6Cl_{14}C$, and $Zr_6Cl_{15}N$[6] constitute an isoelectronic series.

An important structural feature that pertains to such a series is the evident necessity to bond an outer halide ($X^a$) (or other base) to the terminal or exo positions at all six metal vertices of the cluster. This functionality generates most of the structural variations among the different phase types as some combination of the 12 halides within the cluster ($X^i$) and additional outer halides ($X^a$) are employed to fulfill this bonding requirement, viz., as $X^{i-a}$ (and the complementary $X^{a-i}$) in which inner halide in one cluster is outer in another, as the intermediate $X^{a-a}$ that bridge between clusters, or as $X^a$, which is terminal to only one cluster. In most cases this means structural connectivities can be represented as

$$Zr_6X^i_{12-m}X^{i-a}{}_mX^{a-a}{}_{n-p}X^a{}_p$$

with $m + 2(n - p) + p = 6$, although generally only two types of bridging halide functionalities occur simultaneously. The different arrangements possible produce a considerable variety of interlinked cluster networks except that the end member $Zr_6X_{12}X^a_6$ ($n = 6$) contains only isolated cluster anions.

Finally, a decrease in the valence electron count of the selected interstitial Z often produces yet another variation, a reduction of the cluster through a simultaneous addition of one or more cations within the structural framework, for example, in $KZr_6Cl_{14}B$ compared with $Zr_6Cl_{14}C$. Such a change may or may not alter the details of the structural network or the space group relative to those of the analogous cation-free phase.

One particularly versatile group has turned out to be the three-dimensional cluster networks $M_6X^i_{12}X^{a-a}_{6/2}$ with compositions $M_6X_{15}$. These exhibit altogether four different structural frameworks, and all have been realized with various zirconium chlorides. Two different frameworks in this class have been known for sometime for the classical empty cluster phases $Ta_6Cl_{15}$[7] and $Nb_6F_{15}$.[8] More recently, a series of eight zirconium compounds exemplified by $KZr_6Cl_{15}C$ and $CsKZr_6Cl_{15}B$[5] have been obtained with a third $M_6X_{15}$ arrangement, that of $CsNb_6Cl_{15}$.[9] Although these three $M_6X_{15}$ structure types are all related by a common local connectivity, they show a diversity in their structural chemistry in virtually every other aspect: from the local geometry around the intercluster bridging $X^{a-a}$ atoms, which may exhibit all bent or all linear bridges or a combination thereof, to the accommodation of a variety of cations within the $M_6X_{15}$ framework and to the larger three-dimensional connectivity of the structure.

The diversity of this group is enhanced by two new compounds reported here, $K_2Zr_6Cl_{15}B$ and $K_3Zr_6Cl_{15}Be$, which represent still another structural variation in the $M_6X_{15}$ family. Both structures show a combination of structural features found in the other three types of cluster frameworks, and yet they are unrelated to any of them in a larger three-dimensional sense. Interestingly, however, $K_2Zr_6Cl_{15}B$ and $K_3Zr_6Cl_{15}Be$ are related to one another in this three-dimensional connectivity, such that the structure of the latter and room for the third cation can be generated by a distortion of that of the former.

## Experimental Section

The materials utilized, the general synthetic techniques utilizing sealed Ta containers, Guinier powder diffraction and cell parameter refinement methods, otherwise uncited crystallographic programs for adsorption correction, refinement (ALLS, FOUR), etc., and the sources of the scattering factors (which included real and imaginary components of anomalous dispersion) were as referenced or described before.[5,10]

(1) Ziebarth, R. P.; Corbett, J. D. *J. Am. Chem. Soc.* **1985**, *107*, 4571.
(2) Smith, J. D.; Corbett, J. D. *J. Am. Chem. Soc.* **1985**, *107*, 5704.
(3) Smith, J. D.; Corbett, J. D. *J. Am. Chem. Soc.* **1986**, *108*, 1927.
(4) Hughbanks, T. R.; Rosenthal, G.; Corbett, J. D. *J. Am. Chem. Soc.* **1986**, *108*, 8289.
(5) Ziebarth, R. P.; Corbett, J. D. *J. Am. Chem. Soc.* **1987**, *109*, 4844.
(6) Ziebarth, R. P.; Corbett, J. D., to be submitted for publication.
(7) Bauer, D.; von Schnering, H.-G. *Z. Anorg. Allg. Chem.* **1968**, *361*, 259.
(8) Schäfer, H.; Schnering, H.-G.; Niehues, K.-J.; Nieder-Vahrenholz, H. G. *J. Less-Common Met.* **1965**, *9*, 95.
(9) Imoto, H.; Simon, A., unpublished research.

0002-7863/88/1510-1132$01.50/0 

**Table I.** Lattice Parameters of Compounds of the $K_2Zr_6Cl_{15}B$ and $K_3Zr_6Cl_{15}Be$ Structure Types[a]

| compound | a | b | c | β | V |
|---|---|---|---|---|---|
| $K_2Zr_6Cl_{15}B$[b] | 11.386 (1) | 15.980 (1) | 14.008 (1) | 90.0 | 2548.6 (4) |
| $K_2Zr_6Cl_{15}Be$[b] | 11.446 (1) | 16.108 (3) | 14.097 (1) | 90.0 | 2599.1 (6) |
| $K_3Zr_6Cl_{15}Be$[c] | 16.372 (2) | 11.396 (2) | 14.071 (1) | 92.74 (1) | 2622.2 (6) |
| $Rb_3Zr_6Cl_{15}Be$[c] | 16.473 (2) | 11.555 (1) | 14.083 (2) | 93.14 (1) | 2676.6 (6) |

[a] Determined from 35–61 indexed reflections in the Guinier powder diffraction pattern. Axial lengths are in angstroms, and cell volumes, in cubic angstroms. [b] $K_2Zr_6Cl_{15}B$ structure, orthorhombic (*Cccm*). [c] $K_3Zr_6Cl_{15}Be$ structure, monoclinic (*C*2/*c*).

**Synthesis.** The phase $K_2Zr_6Cl_{15}B$ in a new structure type was initially obtained as the major product from a reaction designed to explore the limits of stability of the $CsKZr_6Cl_{15}B$ structure type with different pairs of cations. The reaction was loaded with stoichiometric amounts of Zr powder, $ZrCl_4$, KCl, and amorphous boron powder and was run at 850 °C for 29 days before being air-quenched. The dark-red, crystalline material appeared to be single phase, and the yield was estimated to be greater than 95% on the basis of its Guinier powder pattern, which agreed completely in positions and intensities with the pattern calculated for the structure subsequently determined. A significant autogenous pressure of $ZrCl_4$ exists over the product at temperature, and the slightly reducing conditions created by this loss appear to facilitate the formation of $K_2Zr_6Cl_{15}B$ rather than $KZr_6Cl_{14}B$ and $K_2ZrCl_6$. It is important to note that only $ZrCl_3$ is obtained from analogous reactions in which the interstitial B, Be, etc., has been omitted, except that occasional traces of cluster phases stabilized by adventitious impurities such as carbon and nitrogen may also occur.[2,6]

The isostructural 13-electron cluster $K_2Zr_6Cl_{15}Be$ was prepared from stoichiometric amounts of zirconium powder, $ZrCl_4$, KCl, and Be flakes at 800–850 °C over a 2–3-week period. Yields near 95% were often achieved. As with other 13-electron zirconium chloride clusters, the autogenous $ZrCl_4$ pressure over $K_2Zr_6Cl_{15}Be$ at reaction temperature is somewhat larger than for the more reduced 14-electron cluster compounds. Also, $K_2Zr_6Cl_{15}Be$ is often found as a minor product in preparations of $KZr_6Cl_{13}Be$.[6]

The new composition $K_3Zr_6Cl_{15}Be$ was prepared when the synthesis of $K_4Zr_6Cl_{16}Be$ was attempted by the direct reaction of stoichiometric quantities of Zr powder, $ZrCl_4$, KCl, and Be flakes at 800 °C. The reaction, which was quenched after 21 days, contained a mixture of the dark red $K_3Zr_6Cl_{15}Be$ and white $K_2ZrCl_6$. The analogous $Rb_3Zr_6Cl_{15}Be$ forms under similar conditions. Both compounds can be obtained in ~95% yield. Crystals of $K_3Zr_6Cl_{15}Be$ or $Rb_3Zr_6Cl_{15}Be$ were often formed severely intergrown, although single crystals large enough for X-ray diffraction work could be found or chipped from the intergrown mass.

Partial occupancy of the cation sites does not appear to occur, at least in the case of $K_3Zr_6Cl_{15}Be$. A reaction designed to make $K_{2.5}Zr_6Cl_{15}Be$ instead yielded an approximately 50:50 mixture of $K_2Zr_6Cl_{15}Be$ and $K_3Zr_6Cl_{15}Be$. Lattice parameters of the $K_3Zr_6Cl_{15}Be$ component were not significantly different from those measured for material prepared with excess KCl.

Lattice parameters of the compounds prepared in the $K_2Zr_6Cl_{15}B$ and $K_3Zr_6Cl_{15}Be$ structure types are given in Table I.

**Crystallography.** X-ray diffraction data for $K_2Zr_6Cl_{15}B$ and $K_3Zr_6Cl_{15}Be$ were collected at room temperature from small, dark red, rectangular prisms of the compounds by monochromatic Mo Kα radiation and variable-rate ω-scans on a Syntex diffractometer. The orthorhombic and monoclinic cells chosen for $K_2Zr_6Cl_{15}B$ and $K_3Zr_6Cl_{15}Be$, respectively, were derived from sets of tuned low-angle reflections with the program BLIND.[11] Axial photographs taken on the diffractometer were consistent with the calculated cells in terms of both layer spacings and Laue symmetry. Pertinent data collection details are given in Table II.

**$K_2Zr_6Cl_{15}B$.** The space group symmetry of *Cccm* was chosen on the basis of the observed systematic extinctions and an assumed centricity that was supported by a Wilson plot and later confirmed by the structural refinement. The initial atomic coordinates were determined by direct methods with the program MULTAN 80.[12] Four randomly oriented octahedral zirconium clusters were included as input to aid in the normalization process. An earlier attempt to solve the structure by direct methods without "molecular fragments" had given only a partial solution ($Zr_4$ butterflies), and a complete solution could not be found because of an incorrect assignment of the origin. The correct solution obtained with the inclusion of the molecular fragments translated the origin by ($^1/_4$, $^1/_4$, 0) and gave octahedral $Zr_6$ clusters.

**Table II.** Summary of Crystallographic Data for $K_2Zr_6Cl_{15}B$ and $K_3Zr_6Cl_{15}Be$

| compd | $K_2Zr_6Cl_{15}B$ | $K_3Zr_6Cl_{15}Be$ |
|---|---|---|
| space gp | *Cccm* | *C*2/*c* |
| *Z* | 4 | 4 |
| *a*,[a] Å | 11.386 (1) | 16.372 (2) |
| *b*, Å | 15.980 (1) | 11.396 (2) |
| *c*, Å | 14.008 (1) | 14.071 (1) |
| β, deg | 90.0 | 92.74 (1) |
| cryst dimens, mm | 0.20 × 0.13 × 0.35 | 0.15 × 0.20 × 0.20 |
| 2θ(max), deg | 55.0 | 55.0 |
| octants | *h*,*k*,±*l* | *h*,±*k*,±*l* |
| no. of measd reflcns | 2925 | 12 192 |
| no. of obsd reflcns | 1772 | 5232 |
| no. of indep reflcns | 977 | 2651 |
| *R*(av), % | 1.9 | 2.6 |
| μ, $cm^{-1}$ (Mo Kα) | 41.7 | 42.1 |
| transmissn coeff range | 0.73–1.00 | 0.78–1.00 |
| secondary ext coeff | 1.4 (2) × $10^{-4}$ | 7 (6) × $10^{-7}$ |
| $R$,[b] % | 3.3 | 4.8 |
| $R_w$,[c] % | 4.1 | 3.2 |

[a] Guinier powder diffraction data. [b] $R = \sum||R_o| - |F_c||/\sum|F_o|$. [c] $R_w = [\sum w(|F_o| - |F_c|)^2/\sum w|F_o|^2]^{1/2}$.

The electron density map was initially calculated by Fourier synthesis with only the two "heaviest" atoms obtained from MULTAN 80, which were assumed to be Zr atoms. Successive cycles of least-squares refinement and electron density map calculations with $w(F_o) = \sigma_{F_o}^{-2}$ located the remaining atoms in the structure and identified the composition as $K_2Zr_6Cl_{15}B$. The expected boron interstitial atom was included in the refinement after an approximately 5-electron residual was observed at the cluster center following isotropic refinement of all other atoms. The refinement converged to $R = 0.033$ and $R_w = 0.041$ after application of a secondary extinction correction and a reweighting of the data set to allow for the fact that greater differences in $w(|F_o| - |F_c|)^2$ occurred for small $F_o$. The occupancies of B, K1, and K2 refined along with all other variables to 0.99 (7), 0.99 (1), and 0.92 (2), respectively. The final difference map was flat to less than ±0.4 e/Å$^3$.

The K2 atom occupies a site of $\bar{2}/m$ symmetry and shows a somewhat elongated thermal ellipsoid in the $\vec{b}$ direction, with 0.3-electron peaks at each end in the final difference map. The elongation is apparently a consequence of the local chlorine environment, which provides a long cylindrical cavity similar in many respects to the Cs2 site in $CsKZr_6Cl_{15}B$.[5] A reduction in symmetry to monoclinic seemed unwarranted on the basis of the mirror symmetry seen in the axial photographs, the excellent data averaging (Table II), and the quality of the refinement. A refinement of the structure was attempted in the monoclinic space group *C*2/*c*, however, to look for signs of the type of distortion described below for $K_3Zr_6Cl_{15}Be$ (the $\vec{a}$ and $\vec{b}$ axes of the orthorhombic cell are interchanged in *C*2/*c*). But refinement of all but the K2 atom positional variables under the reduced symmetry conditions showed no deviation from the orthrhombic symmetry of *Cccm*.

**$K_3Zr_6Cl_{15}Be$.** The monoclinic space group *C*2/*c* was chosen on the basis of the observed systematic extinctions and was later confirmed by the successful refinement of the structure in this space group. Three zirconium positions were found by direct methods,[12] while the remainder of the atoms in the structure were located in subsequent Fourier maps. The Be atom was included in the model after an approximately 3-electron residual in the cluster center was seen following isotropic refinement of the Zr, Cl, and K atoms. Simultaneous refinement of both the occupancy of the Be site and its thermal parameter *B* as the process approached the final convergence gave values of 1.08 (5) and 1.5 (3), respectively. The occupancy of K1 refined to 0.999 (7) and K2 to 1.00 (1). The final residual factors for the structural refinement following a correction for secondary extinction and a reweighting of the data set as before were $R = 0.048$ and $R_w = 0.032$.

(10) Hwu, S.-J.; Corbett, J. D.; Poeppelmeier, K. R. *J. Solid State Chem.* **1985**, *57*, 43.
(11) Jacobson, R. A. U.S. AEC Report IS-3469; U.S. Government Printing Office: Ames, IA, 1974.
(12) Main, P.; Fiske, S. J.; Hull, S. E.; Lessinger, L.; Germain, G.; Declerc, J.-P.; Woolfson, M. M. *MULTAN 80. A System of Computer Programs for the Automatic Solution of Crystal Structures from X-ray Diffraction Data*; Department of Physics, University of York: York, England, 1980.

**Table III.** Positional Parameters for $K_2Zr_6Cl_{15}B$

| atom | x | y | z |
|---|---|---|---|
| Zr1 | 0.86207 (9) | 0.13199 (6) | 1/2 |
| Zr2 | 0.36805 (5) | 0.19108 (4) | 0.11677 (4) |
| Cl1 | 0.5078 (2) | 0.3173 (1) | 0.1261 (1) |
| Cl2 | 0.2517 (2) | 0.0545 (1) | 0.1290 (1) |
| Cl3 | 1/4 | 1/4 | 0.2557 (2) |
| Cl4 | 0.5121 (2) | 0.1232 (2) | 0 |
| Cl5 | 0 | 0 | 0 |
| Cl6 | 1/2 | 0.1217 (2) | 1/4 |
| K1[a] | 1/2 | 1/2 | 1/4 |
| K2[b] | 1/4 | 3/4 | 0 |
| B[c] | 1/4 | 1/4 | 0 |

[a] Occupancy refined to 0.99 (1). [b] Occupancy refined to 0.92 (2). [c] Occupancy refined to 0.99 (7).

**Table IV.** Positional Parameters for $K_3Zr_6Cl_{15}Be$

| atom | x | y | z |
|---|---|---|---|
| Zr1 | 0.13369 (3) | 0.13509 (4) | 0.49888 (3) |
| Zr2 | 0.30275 (3) | 0.14997 (4) | 0.63509 (3) |
| Zr3 | 0.68798 (3) | 0.11323 (4) | 0.09790 (4) |
| Cl1 | 0.81105 (9) | 0.0324 (1) | 0.6017 (1) |
| Cl2 | 0.55011 (8) | 0.2270 (1) | 0.1027 (1) |
| Cl3 | 0.26559 (9) | 0.2165 (1) | 0.24632 (9) |
| Cl4 | 0.37599 (9) | 0.0091 (1) | 0.0409 (1) |
| Cl5 | 0 | 0 | 0 |
| Cl6 | 0.37684 (9) | 0.9534 (1) | 0.2891 (1) |
| Cl7 | 0.32483 (8) | 0.4843 (1) | 0.3530 (1) |
| Cl8 | 0.06513 (9) | 0.2234 (1) | 0.3478 (1) |
| K1[a] | 0 | 0.0615 (3) | 3/4 |
| K2[b] | 0.1140 (1) | 0.2448 (1) | 0.0674 (1) |
| Be[c] | 3/4 | 1/4 | 0 |

[a] Occupancy refined to 0.999 (7). [b] Occupancy refined to 1.00 (1). [c] Occupancy refined to 1.08 (5).

**Table V.** Bond Distances in $K_2Zr_6Cl_{15}B$ (Å)

| | occurrence[a] | distance | | occurrence[a] | distance |
|---|---|---|---|---|---|
| | Zr–Zr | | | Zr–Cl$^{a-a}$ | |
| Zr1–Zr2 | 4 | 3.230 (1) | Zr1–Cl5 | 2 | 2.630 (1) |
| Zr1–Zr2 | 4 | 3.267 (1) | Zr2–Cl6 | 4 | 2.640 (1) |
| Zr2–Zr2 | 2 | 3.271 (1) | | | |
| Zr2–Zr2 | 2 | 3.282 (1) | | K–Cl | |
| $\bar{d}$ | | 3.253 | K1–Cl1 | 4 | 3.397 (2) |
| | | | K1–Cl2 | 4 | 3.441 (2) |
| | Zr–B | | K1–Cl5 | 2 | 3.5020 (3) |
| Zr1–B | 2 | 2.277 (1) | $\bar{d}$ | | 3.436 |
| Zr2–B | 4 | 2.3170 (6) | K2–Cl4 | 2 | 3.383 (3) |
| $\bar{d}$ | | 2.304 | K2–Cl3 | 2 | 3.422 (2) |
| | | | K2–Cl1 | 4 | 3.447 (2) |
| | Zr–Cl$^{i}$ | | $\bar{d}$ | | 3.425 |
| Zr1–Cl1 | 4 | 2.555 (2) | | | |
| Zr1–Cl2 | 4 | 2.546 (2) | | | |
| Zr2–Cl1 | 4 | 2.573 (2) | | | |
| Zr2–Cl2 | 4 | 2.559 (2) | | | |
| Zr2–Cl3 | 4 | 2.546 (2) | | | |
| Zr2–Cl4 | 4 | 2.558 (2) | | | |

[a] The number of times the distance occurs per cluster or cation.

**Table VI.** Bond Distances in $K_3Zr_6Cl_{15}Be$ (Å)

| | occurrence[a] | distance | | occurrence[a] | distance |
|---|---|---|---|---|---|
| | Zr–Zr | | | Zr–Cl$^{a-a}$ | |
| Zr1–Zr2 | 2 | 3.2900 (8) | Zr1–Cl5 | 2 | 2.6767 (6) |
| Zr1–Zr2 | 2 | 3.2948 (8) | Zr2–Cl6 | 2 | 2.703 (1) |
| Zr1–Zr3 | 2 | 3.2895 (8) | Zr3–Cl6 | 2 | 2.670 (2) |
| Zr1–Zr3 | 2 | 3.2923 (8) | | | |
| Zr2–Zr3 | 2 | 3.3155 (8) | | K–Cl | |
| Zr2–Zr3 | 2 | 3.3158 (7) | K1–Cl2 | 2 | 3.307 (3) |
| $\bar{d}$ | | 3.2997 | K1–Cl7 | 2 | 3.316 (2) |
| | | | K1–Cl5 | 2 | 3.5869 (7) |
| | Zr–Be | | K1–Cl1 | 2 | 3.663 (2) |
| Zr1–Be | 2 | 2.3104 (5) | K1–Cl8 | 2 | 3.665 (3) |
| Zr2–Be | 2 | 3.3456 (5) | $\bar{d}$ | | 3.508 |
| Zr3–Be | 2 | 3.3435 (5) | | | |
| $\bar{d}$ | | 2.3332 | K2–Cl6 | 1 | 3.118 (2) |
| | | | K2–Cl4 | 1 | 3.200 (2) |
| | Zr–Cl$^{i}$ | | K2–Cl8 | 1 | 3.227 (2) |
| Zr1–Cl7 | 2 | 2.554 (1) | K2–Cl7 | 1 | 3.311 (2) |
| Zr1–Cl8 | 2 | 2.562 (2) | K2–Cl5 | 1 | 3.463 (2) |
| Zr1–Cl1 | 2 | 2.566 (2) | K2–Cl3 | 1 | 3.465 (2) |
| Zr1–Cl2 | 2 | 2.582 (2) | K2–Cl2 | 1 | 3.526 (2) |
| Zr2–Cl3 | 2 | 2.555 (1) | K2–Cl1 | 1 | 3.647 (2) |
| Zr2–Cl4 | 2 | 2.575 (2) | $\bar{d}$ | | 3.370 |
| Zr2–Cl7 | 2 | 2.601 (1) | | | |
| Zr2–Cl8 | 2 | 2.602 (2) | | | |
| Zr3–Cl3 | 2 | 2.571 (1) | | | |
| Zr3–Cl4 | 2 | 2.581 (2) | | | |
| Zr3–Cl2 | 2 | 2.607 (1) | | | |
| Zr3–Cl1 | 2 | 2.609 (2) | | | |

[a] The number of times the distance occurs per cluster or cation.

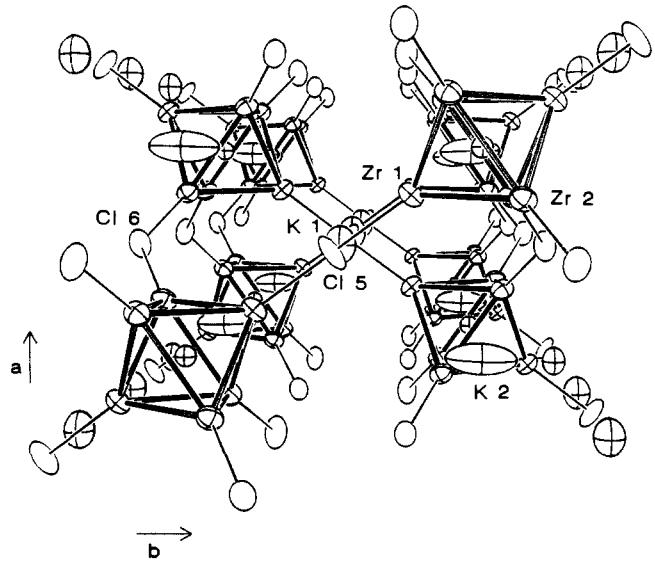


**Figure 1.** Approximate [00$\bar{1}$] view of the structure of $K_2Zr_6Cl_{15}B$ with Cl$^{i}$ atoms omitted for clarity. The $Zr_6B$ clusters are outlined. Cl$^{a-a}$ atoms are drawn as open ellipsoids and K atoms as crossed ellipsoids. Thermal ellipsoids are at 90% probability level.

## Structural Results and Discussion

Atomic coordinates for $K_2Zr_6Cl_{15}B$ and $K_3Zr_6Cl_{15}Be$ appear in Tables III and IV, respectively, while thermal parameters and structure factor amplitudes are tabulated in the supplementary material.

The structures of $K_2Zr_6Cl_{15}B$ and $K_3Zr_6Cl_{15}Be$, like that of $KZr_6Cl_{15}C$,[5] show a combination of bent and linear Cl$^{a-a}$ bridges between cluster units. Unlike $KZr_6Cl_{15}C$, however, both $K_2Zr_6Cl_{15}B$ and $K_3Zr_6Cl_{15}Be$ can be viewed in terms of only linear chains of a single cluster type that are interconnected into a three-dimensional array by additional bent Cl$^{a-a}$ bridges. Thus, one-third of the intercluster Cl$^{a-a}$ bridges are linear compared with one-sixth in $KZr_6Cl_{15}C$, etc. Important differences also exist between $K_2Zr_6Cl_{15}B$ and $K_3Zr_6Cl_{15}Be$. Bonding distances in $K_2Zr_6Cl_{15}B$ and $K_3Zr_6Cl_{15}Be$ are tabulated in Tables V and VI, respectively.

**$K_2Zr_6Cl_{15}B$.** The linear chains of bridged clusters in $K_2Zr_6Cl_{15}B$ are packed to give a crosscrossing pattern of chains when viewed down the $\vec{c}$ axis, as shown in Figure 1. The crisscrossing linear chains intersect in projection at an angle of ~109°. The Zr–Cl$^{a-a}$–Zr bridge in the linear cluster chain is constrained to linearity by the crystallographically imposed $2/m$ symmetry of the Cl$^{a-a}$ site, while the angle at the bent Cl6 bridges is 130.3 (1)°. Interestingly, the linear chain is actually very slightly puckered, however, because the Cl$^{a-a}$–Zr bond in the linear bridge comes into the cluster 2.6° off axis; i.e., the Cl$^{a-a}$–Zr–B angle is 177.40 (5)°. Similar deviations from linearity for Cl$^{a-a}$–Zr–Z are observed in practically all other cluster network compounds. In this case the deviation may play a role in relieving what appears to be a

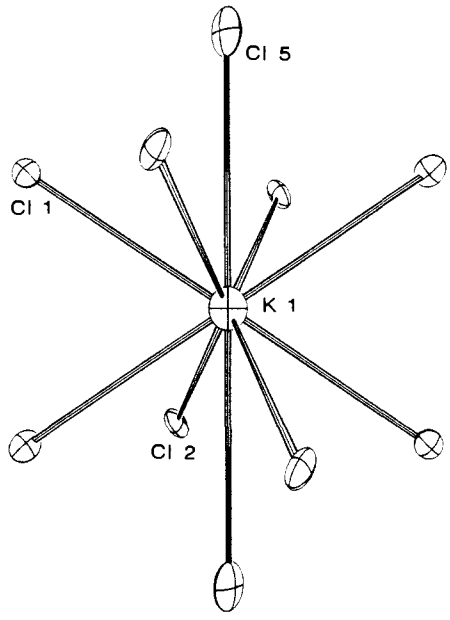


**Figure 2.** Local chlorine environment around K1 in $K_2Zr_6Cl_{15}B$. The site has 222 symmetry with twofold axes running vertically and horizontally in the figure and perpendicular to the page. Thermal ellipsoids are drawn at 50% probability.

compression down the linear chain that is also suggested by the slightly flattened ellipsoid obtained for Cl5. No tilting of the clusters is allowed in $KZr_6Cl_{15}C$ and $CsKZr_6Cl_{15}B$ where a higher effective crystallographic symmetry is imposed, but a more severe flattening of the thermal ellipsoids of the atoms in the chain is seen instead, particularly for the intercluster bridging $Cl2^{a-a}$ atom.[5]

The potassium atoms in $K_2Zr_6Cl_{15}B$ reside in two crystallographically distinct sites. The K1 atom lies between adjacent linearly bridging $Cl^{a-a}$ atoms and on a twofold axis parallel to $\vec{c}$. The atoms are arranged to give infinite strings of $\cdots Cl5^{a-a}$–K1–$Cl5^{a-a}$–K1$\cdots$ down the edges and center of the cell in the $\vec{a}$ direction (Figure 1). The local environment of K1 shown in Figure 2 consists of ten chlorine atoms, two $Cl^{a-a}$, and eight $Cl^{i}$, forming a polyhedron with 222 symmetry ($D_{2d}$) that can be visualized as a distorted bicapped square antiprism. The K–Cl distances are typical, averaging 0.04 Å greater than the sum of crystal radii.[13]

The more unusual site available to K2 lies midway between $[Zr_6Cl^{i}_{12}B]$ clusters along $\vec{c}$. The site has $2/m$ symmetry and is bounded by eight inner chlorine atoms at comparable distances but in the form of a highly elongated trigonal antiprism, with two of the long edges of the antiprism bridged in a trans fashion by Cl3 atoms (Figure 3). This can alternately be viewed as a rigorously planar hexagonal array of Cl1 and Cl3 atoms about K2, with Cl4 atoms above and below that are considerably displaced from the normal. This arrangement is remarkably similar to that around the Cs2 site in $CsKZr_6Cl_{15}B$.[5] Just as in the latter, the K2 atom is elongated toward opposite faces of the antiprism in the $\vec{b}$ direction, apparently in response to the structural framework since nearest chlorine neighbors in that direction are over 5 Å away. The ratios of the principal axes are less extreme in the case of K2, however, 1:5.3:1.7.

The $Zr_6Cl_{15}B$ cluster has crystallographically imposed $2/m$ ($C_{2h}$) symmetry. The two triangular metal faces perpendicular to $\vec{a}$ are nearly equilateral but have been displaced with respect to one another to give four shorter (3.23 Å) and two longer (3.28 Å) interlayer Zr–Zr distances per cluster. This may reflect strain in the framework. The average Zr–Zr distance of 3.253 Å is typical of boron-centered chloride clusters. A calculated effective boride crystal radius of 1.44 Å can be obtained by subtracting the tabulated 0.86-Å value for the six-coordinate metal from the average Zr–B distance of 2.304 Å. This Zr–B distance is 0.08 Å less than the average observed in $CsZr_6I_{14}B$[3] where an iodine matrix effect might be expected to operate.

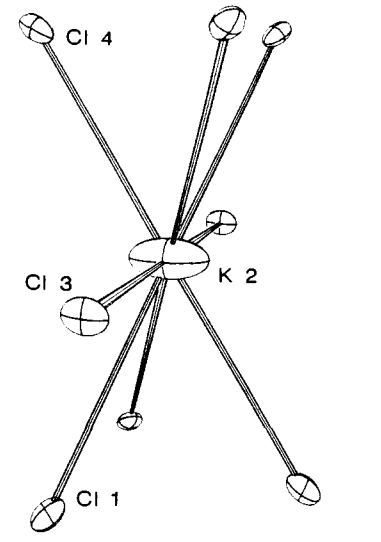


**Figure 3.** Chlorine environment around K2 in $K_2Zr_6Cl_{15}B$. The site has $2/m$ symmetry with Cl3 and K2 on the axis and the mirror plane containing Cl4 approximately in the plane of the paper. The site is very similar to the Cs2 site in $CsKZr_6Cl_{15}B$.[5] Thermal ellipsoids are drawn at 50% probability.

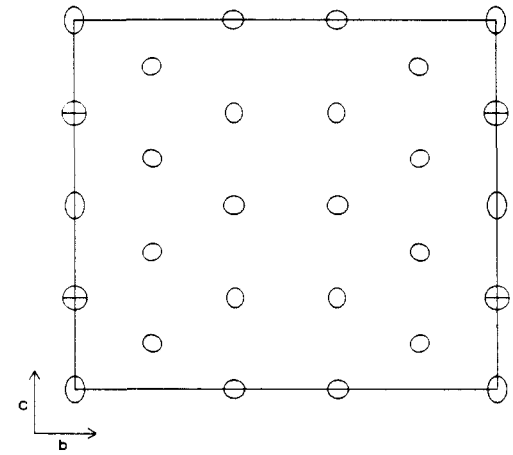


**Figure 4.** [100] projection on $x = 0$ of the modified close-packed layer of atoms in $K_2Zr_6Cl_{15}B$ designated A′. A square net where strips of close-packed atoms come together runs down the center of the projection. The open ellipses are chlorine atoms, and the crossed ellipses, K1 atoms.

An alternative approach to the structure of $K_2Zr_6Cl_{15}B$ is to view it as a close-packed array of chlorine layers with an ordered occupancy of octahedral sites between layers by zirconium. The chlorine layers, some of which are clearly visible in Figure 1, stack in the $\vec{a}$ direction. However, the individual layers in $K_2Zr_6Cl_{15}B$ are not close-packed, unlike those in several other structures that have been described in terms of close-packed anion layers.[14,15] Rather, two distinct "modified" close-packed nets are seen in $K_2Zr_6Cl_{15}B$. One type of net, designated A′ and A″, contains all of the K1 and $Cl^{a-a}$ (Cl5 and Cl6) and some of the $Cl^{i}$ atoms and is located at $x = 0$ and $^1/_2$. As seen in projection in Figure 4, the A′ layer is composed of vertical strips of approximately close-packed atoms that come together at seams with square packing. The A″ layer at $x = {}^1/_2$ has the same square net seam translated by $\vec{b}/2$. A second modified net designated B′ and B″ (at $\vec{b}/2$) is positioned at $x = {}^1/_4$ and $^3/_4$, respectively; its projection is shown in Figure 5. This net is a formerly close-packed array of atoms that has been expanded ~25% in the $\vec{b}$ (horizontal) direction to form zigzag rifts parallel to $\vec{c}$ between the rows of

(13) Shannon, R. D. *Acta Crystallogr., Sect. A: Cryst. Phys., Diffr., Theor. Gen. Crystallogr.* **1976**, *A32*, 751.

(14) Imoto, H.; Corbett, J. D. *Inorg. Chem.* **1981**, *20*, 145.
(15) Warkentin, E.; Masse, R.; Simon, A. *Z. Anorg. Allg. Chem.* **1982**, *491*, 323.

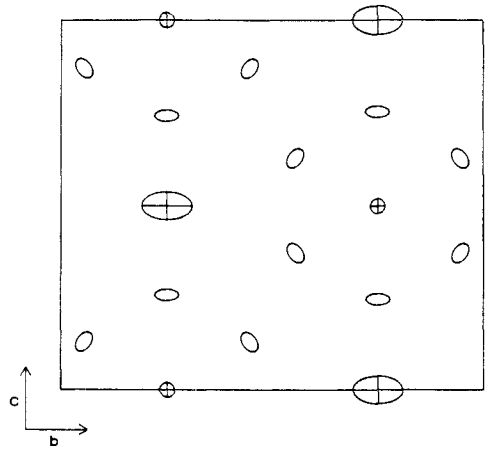


**Figure 5.** [100] projection on $x = {}^1/_4$ of the expanded close-packed layer of atoms designated B′. The small and large crossed ellipses are B and K2, respectively, and the open ellipses, $Cl^1$. The expansion of the layer in the $\vec{b}$ direction is obvious from the four chlorine atoms down the edge and center of the cell ($y \simeq 0.0, 0.5$), which would lie on lines in a close-packed array.

clusters, as seen along the edges and in the center of the figure. Formation of the rifts is necessary for the layer to mesh with zones of square packing in the A layers above and below. The expansion of the layer in the $\vec{b}$ direction is also responsible for the extended K2 cavity between clusters. The stacking of the modified layers in $K_2Zr_6Cl_{15}B$ is ···A′B′A″B″···.

The expansions found in these individual layers, by either the insertion of square-packed zones in A or the formation of rifts between rows of clusters in B, represent a compromise between the needs to accommodate linear intercluster $Cl^{a-a}$ bridges and to maintain reasonable Zr–$Cl^{a-a}$ distances, i.e., matrix effects. As will be seen, room for the second cation is also created in the expansion, and this appears to be the primary driving force for the formation of the linear intercluster $Cl^{a-a}$ bridges. The connection between linear $Cl^{a-a}$ bridges and cation site formation is described in more detail in the Discussion of Framework Relationships.

The description of $K_2Zr_6Cl_{15}B$ as a close-packed layering of chlorine atoms provides a convenient way of visualizing the structure and packing and also allows its relationship to $KZr_6Cl_{14}B$[6] ($CsZr_6I_{14}C$ type[2]) to be seen more easily. The projection of a layer of clusters in $K_2Zr_6Cl_{15}B$ onto $z = {}^1/_4$ at the top of Figure 6 shows a striking resemblance to an analogous projection onto $z = {}^1/_2$ in $KZr_6Cl_{14}B$ shown below. The basic arrangement of clusters within the layer is identical in the two compounds except that clusters in every other row in $K_2Zr_6Cl_{15}B$ have been rotated 180° around an axis perpendicular to the layer. The stacking of the cluster layers is the same in both compounds with the next layer translated by $\vec{b}/2$. The cation position in $KZr_6Cl_{14}B$ also clearly carries over into that for K2 in the $K_2Zr_6Cl_{15}B$ structure. The rifts in the $K_2Zr_6Cl_{15}B$ cluster layer can be easily visualized as a result of an expansion of the $KZr_6Cl_{14}B$ cluster layer. The reorientation of every other row of clusters and the expansion of the cluster layer are both consequences of the replacement of $Cl^{a-i}$ connectivity in $KZr_6Cl_{14}B$ with linear $Cl^{a-a}$ intercluster connectivity. These in turn can be understood in terms of the need to create a second cation site on conversion of the $KZr_6Cl_{14}B$ type structure to $K_2Zr_6Cl_{15}B$ type through the above process.

The $K_2Zr_6Cl_{15}B$ structure is also more distantly related to $CsKZr_6Cl_{15}B$. The transformation of $CsKZr_6Cl_{15}B$ to $K_2Zr_6Cl_{15}B$ involves the linearization of the zigzag cluster chain (which requires an extensive breaking and re-formation of Zr–$Cl^{a-a}$ bonds) and translations of the linear cluster chains in the chain direction. The details of the transformation are somewhat tedious and not particularly educational. Of interest, however, is the transformation of the cation sites from one structure to the other. The Cs1 and Cs2 sites in $CsKZr_6Cl_{15}B$ transform to one equivalent site with Cs2 character that accommodates K2. The potassium site carries over largely unchanged to that for K1. The notable

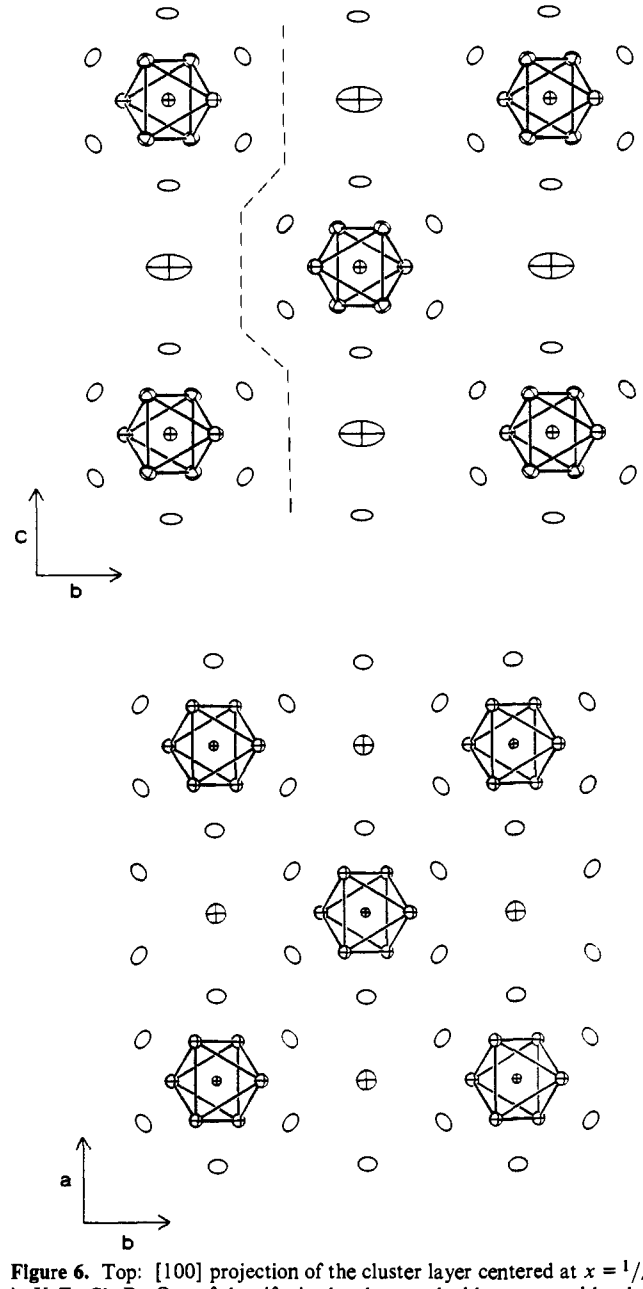


**Figure 6.** Top: [100] projection of the cluster layer centered at $x = {}^1/_4$ in $K_2Zr_6Cl_{15}B$. One of the rifts in the close-packed layer caused by the expansion in $\vec{b}$ is marked by the dashed line. Particular attention should be paid to the orientation of the clusters with respect to one another and the elongation of the K2 site in the $\vec{b}$ direction. Bottom: [001] projection of the clusters and a close-packed layer in $KZr_6Cl_{14}B$[2,6] centered at $z = {}^1/_2$. The crossed ellipsoids from largest to smallest mark K, Zr, and B, respectively. Note that all clusters are oriented in the same manner.

similarity of the two types of sites can be seen by a comparison with ref 5.

**$K_3Zr_6Cl_{15}Be$.** The structure of monoclinic $K_3Zr_6Cl_{15}Be$ shown in Figure 7 in a view down the $\vec{c}$ axis can be seen to be directly related to the orthorhombic structure of $K_2Zr_6Cl_{15}B$ (Figure 1). As in $K_2Zr_6Cl_{15}B$, the structure is composed of a crisscrossing network of linear cluster chains connected into a three-dimensional array by additional bent $Cl^{a-a}$ bridges. Room for a third cation has been created by a small monoclinic distortion of the lattice that splits the former K2 ($2/m$) site in $K_2Zr_6Cl_{15}B$ into two inversion-related sites that have no crystallographically imposed symmetry. The details of the monoclinic distortion include a slight displacement of the linear cluster chains with respect to one another in the $\vec{b}$ direction ($K_2Zr_6Cl_{15}B$ axes), a result of the 2.7° increase in the monoclinic angle ($\alpha$ in $K_2Zr_6Cl_{15}B$), and an approximately 7° rotation of each linear cluster chain around its axis. The chains at $z = 0$ and ${}^1/_2$ rotate forward and backward,

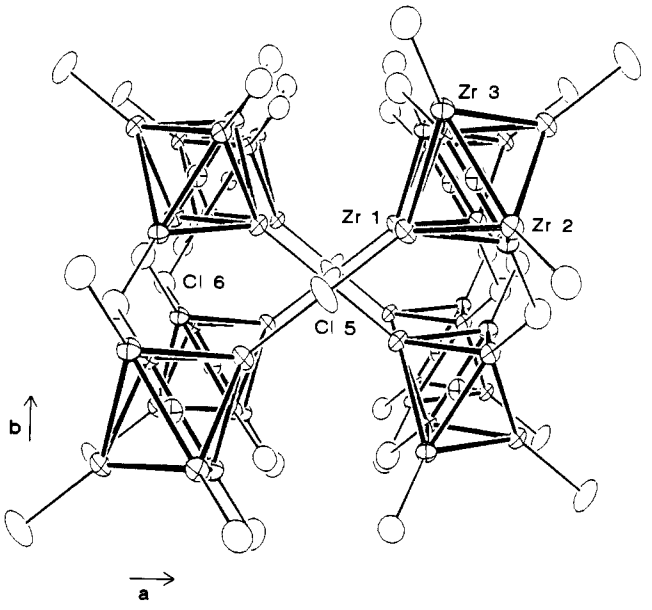


**Figure 7.** Approximate [00$\bar{1}$] view of the three-dimensional cluster framework in $K_3Zr_6Cl_{15}Be$ (90% thermal ellipsoids). The $Cl^i$ and K atoms have been omitted for clarity. The $Zr_6$ clusters are drawn in heavy lines and are centered by beryllium atoms. Rotation of the cluster chains is particularly evident from the up–down row of $Cl^{a-a}$ atoms on the left and right sides of the drawing.

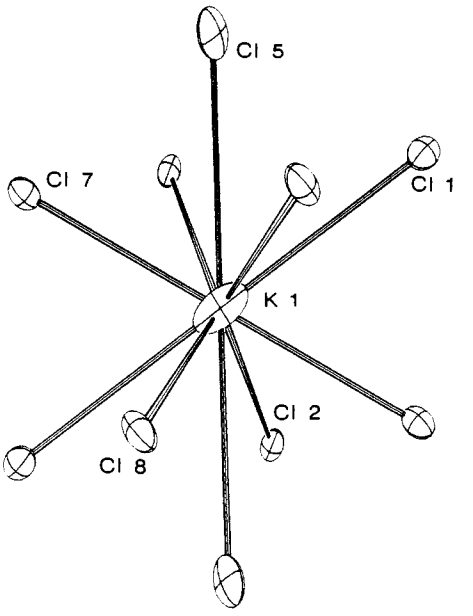


**Figure 8.** Local chlorine environment around K1 in $K_3Zr_6Cl_{15}Be$ viewed along the twofold axis. Thermal ellipsoids are drawn at 50% probability.

respectively, when viewed down $\vec{c}$. This result can be easily seen in the characters of the strings of bent $Cl^{a-a}$ bridges at the left and right sides of Figures 1 and 7. The K1 atoms are displaced 0.7 Å in this process from what were formerly twofold axes parallel to $\vec{c}$ in $K_2Zr_6Cl_{15}B$.[16]

Rotation of the cluster chains, while important in the formation of the third cation site, significantly disrupts the pseudo-close-packed anion layers in $K_2Zr_6Cl_{15}B$. The "layers" in $K_3Zr_6Cl_{15}Be$ are now packed in the $\vec{b}$ direction but are extremely puckered, with a peak-to-valley height of over 1.0 Å. Interestingly, the monoclinic distortion and cation addition appear to have improved the packing efficiency of the cell. Comparison of the cell volumes of $K_2Zr_6Cl_{15}Be$ and $K_3Zr_6Cl_{15}Be$ (Table I) shows a volume change of only 5.8 $Å^3$/K atom, a value nearly 40% less than that expected on the basis of the molar volume increment of 16 $cm^3$ $mol^{-1}$ (9.6 $Å^3$/atom) derived for potassium by Biltz.[17] The simple comparison is not entirely valid, however, because the change from $K_2Zr_6Cl_{15}Be$ to $K_3Zr_6Cl_{15}Be$ involves not only the addition of a third cation but also a 1-electron reduction of the cluster and a concomitant decrease in cluster volume. A rough estimate of the volume change associated with a 13- to 14-electron cluster reduction is 4.4 $Å^3$ (from a comparison of the volume of $Zr_6Cl_{14}B$ and $KZr_6Cl_{14}B$[6] where the $K^+$ cation is approximately the same size as the unoccupied site). Thus the compensated volume change of 10.2 $Å^3$/K is nearly equal to the value predicted and suggests little change in packing efficiency has occurred.

The cluster in $K_3Zr_6Cl_{15}Be$ is larger than that in $K_2Zr_6Cl_{15}B$ simply on the basis of encapsulation of the larger beryllide interstitial. The Zr–Zr distances average 3.300 Å, and the average Zr–Be distance is 2.333 Å, comparable with those in other clusters containing beryllium.[6] The cluster distortion found in $K_2Zr_6Cl_{15}B$ has largely disappeared, although a very slight compression of the $Zr_6Cl_{12}Be$ cluster down the linear chain is observed. The slight puckering of the linear cluster chains associated with the nonlinearity of the $Cl^{a-a}$–Zr–Z bond angle is also nearly gone, with the $Cl5^{a-a}$–Zr1–Be angle now 179.07 (2)°.

The local geometry about the K1 site in $K_3Zr_6Cl_{15}Be$ (Figure 8) is not significantly different from that found in $K_2Zr_6Cl_{15}B$ (Figure 2), and it again shows a strong similarity to the K site in $KZr_6Cl_{15}C$.[5] The displacement of this from the former twofold axis in $K_2Zr_6Cl_{15}B$ and the cluster chain rotations have reduced the site symmetry from 222 to 2 ($D_{2d}$ to $C_2$) and produced a slight lengthening of six and a shortening of four K–Cl distances.

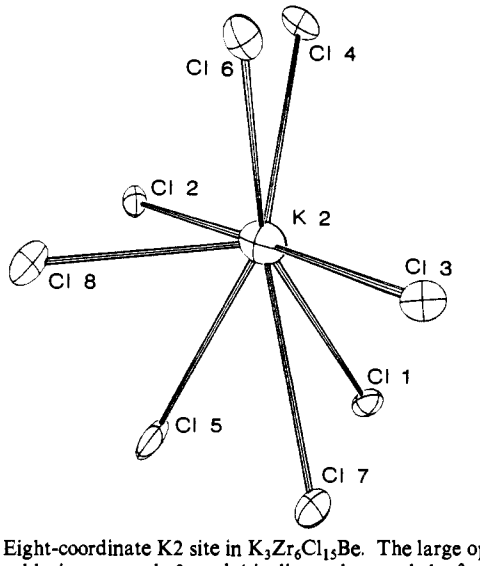


**Figure 9.** Eight-coordinate K2 site in $K_3Zr_6Cl_{15}Be$. The large open face defined by chlorine atoms 1, 3, and 4 is directed toward the former K2 site in $K_2Zr_6Cl_{15}B$ and, beyond, a like new K2 site. Thermal ellipsoids are drawn at 50% probability.

In contrast, the new K2 site is significantly different from the second one in $K_2Zr_6Cl_{15}B$. As shown in Figure 9, this now consists of a somewhat irregularly shaped eight-coordinate site with the large open face Cl1, Cl3, and Cl4. Pairs of these K2 sites facing one another are located on opposite sides of and ~2.2 Å from the former K2 site and between each pair of clusters along $\vec{c}$.

The creation of a pair of K2 sites from the single K2 site in $K_2Zr_6Cl_{15}B$ is fundamentally linked to the rotation of the cluster chains. The K2 site in $K_2Zr_6Cl_{15}B$ is, as one will recall, an elongated trigonal antiprism with two long trans edges bridged by additional chlorine atoms (Figure 3). The thermal ellipsoid of the latter K2 is elongated in the $\vec{b}$ direction toward the distant Cl2 atoms that form the boundaries of the cavity. Rotation of the cluster chains causes a pair of Cl1 atoms in the trigonal antiprism to collapse toward the center of the K2 site. Simultaneously, both ends of the cavity along $\vec{b}$ expand outward to form the new K2 sites. The transformation is schematically diagram-

(16) The crystallographic $\vec{a}$ and $\vec{b}$ axes in $K_2Zr_6Cl_{15}B$ are interchanged on conversion to $K_3Zr_6Cl_{15}Be$ in order to be consistent with the crystallographic convention of a unique monoclinic $\vec{b}$ axis.

(17) Biltz, W. *Raumchemie der festen Stoffe*; L. Voss: Leipzig, Germany, 1935.

**Table VII.** Distribution of $X^{a-a}$ Bridges in $M_6X_{12}X_{6/2}$ Type Structures

| structure type | space gp | $X^{a-a}$ bridge type, % | | criteria | |
|---|---|---|---|---|---|
| | | linear | bent | FBS[a] clusters directly linked[b] | no. of FBS[a] clusters indirectly linked by four-rings[c] |
| $Ta_6Cl_{15}$ | *Ia3d* | 0 | 100 | no | 2 |
| $CsNb_6Cl_{15}$ | *Pmma* | 17 | 83 | yes | 0 |
| $K_2Zr_6Cl_{15}B$ | *Cccm* | 33 | 67 | no | 2, 3 |
| $K_3Zr_6Cl_{15}Be$[d] | *C2/c* | 33 | 67 | no | 2,3 |
| $Nb_6F_{15}$ | *Im3m* | 100 | 0 | no | 4 |

[a] First bonding sphere (FBS); see text. [b] By three-rings, $(-Zr-Zr-Cl^{a-a}-)_3$. [c] Four bridged clusters, $(-Zr-Zr-Cl^{a-a}-)_4$. [d] Variation of the $K_2Zr_6Cl_{15}B$ type; see text.

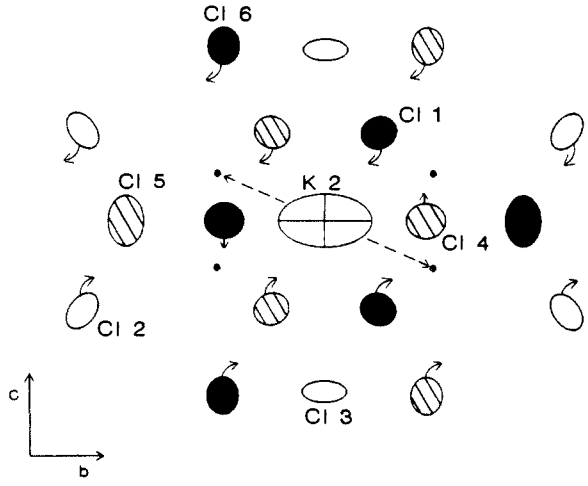


**Figure 10.** [100] projection of the K2 site in $K_2Zr_6Cl_{15}B$ and the atomic displacements associated with the distortion of the site that occur during the conversion to $K_3Zr_6Cl_{15}Be$. The dotted line indicates the directions of K2 motion, and the small circles indicate the final site: ⊛, $y \simeq 1/2$; ○, $y \simeq 1/4$; ●, $y \simeq 0$. Curved arrows to the right indicate movement up, and to the left, down. A twofold axis lies vertical and parallel to $\vec{c}$.

med in projection in Figure 10. A second, energy-equivalent distortion with chain rotations in the opposite directions is related to that shown by the former twofold axis along $\vec{c}$.

### Discussion of Framework Relationships

The interrelationships among the four distinct $(M_6X_{12})/X_{6/2}$ frameworks that have been structurally characterized so far, namely those of the $Ta_6Cl_{15}$,[7] $CsNb_6Cl_{15}$,[9] $K_2Zr_6Cl_{15}B$, and $Nb_6F_{15}$[8] structure types, and the factors that govern their formation are not always readily apparent. However, the ability to obtain all four structure types and variations thereon in a single system, namely the zirconium chlorides, has helped to elucidate some of these interrelationships and formation factors. Although all of the known $M_6X_{15}$ compounds have the same style of local connectivity $[M_6X^i_{12}]X^{a-a}{}_{6/2}$, major structural differences appear in the larger three-dimensional cluster connectivity, the local $Cl^{a-a}$ geometry, and, of course, the lattice symmetry. These details are summarized in Table VII.

When they are viewed as a continuum, the $M_6X_{15}$ structure types create a nicely defined series whose members are differentiated by their local $Cl^{a-a}$ geometry. The $Ta_6Cl_{15}$ structure, which includes the relevant $Zr_6Cl_{15}N$, $Na_{0.5}Zr_6Cl_{15}C$, and the slightly distorted $Na_2Zr_6X_{15}B$ examples,[6] occurs at one end of the series and has only bent $X^{a-a}$ bridges joining clusters, while $Nb_6F_{15}$ and the recently prepared isostructural $Zr_6Cl_{15}Co$[18] are at the opposite end and contain only linear $X^{a-a}$ bridges. The other $M_6X_{15}$ structure types exhibit intermediate combinations of bent and linear $X^{a-a}$ bridges: $CsNb_6Cl_{15}$, $KZr_6Cl_{15}C$, $CsKZr_6Cl_{15}B$, and the like have one-sixth linear $X^{a-a}$ bridges, the remainder bent, while the two structures reported here, $K_2Zr_6Cl_{15}B$ and $K_3Zr_6Cl_{15}Be$, each contain one-third linear bridges. Compounds with larger percentages of linear $X^{a-a}$ bridges have probably not been observed because of the packing inefficiencies associated with the linear bridges. The presence of more and larger cations may provide a way to circumvent this problem.

The need to accommodate a specific number of cations to obtain a preferred electronic state of the cluster and the sizes of the cations are both important factors in differentiating the formation of the various structure types, and it was this factor that forced the formation of the $K_3Zr_6Cl_{15}Be$ structure. In general the introduction of linear $X^{a-a}$ bridges tends to create larger voids within the structure and consequently room for more or larger cations. The trend is nicely illustrated on going from $Ta_6Cl_{15}$ with no linear bridges, to $CsKZr_6Cl_{15}B$ with one-sixth linear bridges, to $K_3Zr_6Cl_{15}Be$ with one-third linear bridges, and finally to $Nb_6F_{15}$ with all linear bridges. The $Ta_6Cl_{15}$ structure presently appears to be limited either to compounds with no cations, such as $Ta_6Cl_{15}$ and $Zr_6Cl_{15}N$, or to those that contain small cations, $Na_{0.5}Zr_6Cl_{15}C$[6] and $Na_xNb_6Cl_{15}$ ($x < 1$)[9] being examples. In contrast, zirconium examples of the $CsNb_6Cl_{15}$ structure have been obtained only in compounds containing one cation as large as potassium or, if with two cations, one at least as large as rubidium. The $K_3Zr_6Cl_{15}Be$ structure with one-third linear $X^{a-a}$ bridges has been found only for compounds that contain three potassium or rubidium cations. Finally, in $Nb_6F_{15}$ the voids created by the linear $X^{a-a}$ bridges have become so large that it is possible or necessary to fill these with a second interpenetrating lattice of $Nb_6F_{15}$ clusters.

The factors that differentiate the formation of the $Ta_6Cl_{15}$ and $Nb_6F_{15}$ structures appear more subtle. The only important difference between $Zr_6Cl_{15}N$[6] and $Zr_6Cl_{15}Co$[18] in the $Ta_6Cl_{15}$ and $Nb_6F_{15}$ structures, respectively, is the size of the interstitial atom and, hence, the proximity of the zirconium atoms to the square faces of the cuboctahedron defined by the 12 edge-bridging $Cl^i$ atoms. This change in the metal atom position suggests the formation of the two structures is probably determined by small differences in bonding and packing efficiencies, with the more ideal clusters, i.e., those with the M atoms nearer the faces formed by the $Cl^i$ atoms, adopting the $Nb_6F_{15}$ structure. The importance of having the M atom near the face is that it allows a reasonable $M-Cl^{a-a}$ bond distance to be maintained while adequate room is left for the second interpenetrating lattice.

Although exhibiting the same local connectivity around each cluster, the structural frameworks of the $Ta_6Cl_{15}$, $CsNb_6Cl_{15}$, $K_2Zr_6Cl_{15}B$, and $Nb_6F_{15}$ types are not related to one another in a larger three-dimensional sense. In other words, none of the four structural frameworks can be interconverted simply by rotation of clusters and bending at bridging chlorine atoms, i.e., without breaking $M-X^{a-a}$ bonds. The inequivalence of the structures can be seen by examining them in light of two criteria, namely (1) whether any of the six clusters in the first bonding sphere (FBS) of a central cluster are directly interconnected through an $X^{a-a}$ atom and (2) if not, how many of the other five about the central unit are indirectly linked to the sixth cluster through one additional cluster excluding, of course, the central cluster that interconnects all six. The first criterion conveniently separates the $CsNb_6Cl_{15}$ structure from the rest since this has directly connected clusters linked to a common central cluster. Described somewhat differently, but nonetheless equivalently, the shortest bonding path through this structure back to a starting point without retracing

(18) Zhang, J.; Corbett, J. D., unpublished research.

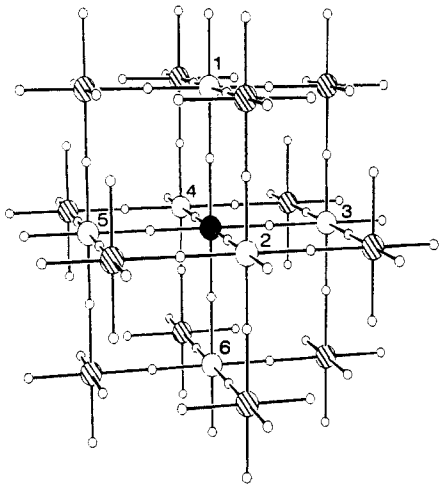


**Figure 11.** Schematic representation of the cluster connectivity in one interpenetrating lattice in $Nb_6F_{15}$. The large filled ellipsoid represents the central $Nb_6F^i_{12}$ cluster, and the small spheres represent bridging $F^{a-a}$ atoms. First-bonding-sphere (FBS) clusters are represented by the large open spheres labeled 1–6, and the cross-hatched spheres indirectly connect FBS clusters.

is $(-Zr-Zr-Cl^{a-a}-)_3$, viz., a three-ring.

In all of the other $M_6X_{15}$ structure types, the shortest path involves four-rings $(-Zr-Zr-Cl^{a-a})_4$; i.e., none of the clusters linked to a common central cluster are directly connected to another. The $Nb_6F_{15}$ structure can be separated from the rest by recognizing that its structural framework is actually two interpenetrating lattices. The inequivalece of the remaining two structures, $Ta_6Cl_{15}$ and $K_2Zr_6Cl_{15}B$, requires the use of the second, more complicated criterion, which is concerned with the indirect interconnectivity of the six clusters joined to a common central cluster. When we start with one of the six first-bonding-sphere (FBS) clusters, the distinguishing feature is the number of the other FBS clusters that are connected to the first through one additional, external cluster. Because all of the clusters in these structures are equivalent by symmetry, the cluster chosen as the central cluster is immaterial.

The concept of the second criterion is illustrated in Figure 11, which shows a schematic representation of the connectivity in one of the interpenetrating lattices in $Nb_6F_{15}$. The central cluster selected is the black sphere, and the first bonding sphere of clusters are the open spheres labeled 1–6. Choosing cluster 1, it is quickly evident it is indirectly connected through one cross-hatched cluster to clusters 2–5, all of which are directly connected to the black central cluster. In other words, each FBS cluster is indirectly connected through one additional cluster to *four* other FBS clusters, namely, to all but the one that is trans. The criterion can also be expressed in terms of circular bonding paths through the structure; specifically, starting at one FBS cluster, how many of the other five FBS clusters are linked to it in $(-N-M-X^{a-a}-)_4$ rings that include the central cluster. The schematic of the connectivity in the $Ta_6Cl_{15}$ structure in Figure 12 illustrates its difference; each cluster in the first bonding sphere is indirectly connected through one external (shaded) cluster to only two other FBS clusters.

The situation in $K_2Zr_6Cl_{15}B$ is slightly different. Here one finds that the number of clusters indirectly connected is dependent on whether the chosen cluster is connected to the central cluster through a linear $Cl^{a-a}$ bridge or a bent one. The schematic of the connectivity in $K_2Zr_6Cl_{15}B$ is illustrated in Figure 13. Clusters *linearly* bridged to the central cluster are indirectly connected to *two* other FBS clusters, while clusters connected through a *bent* $Cl^{a-a}$ bridge ae indirectly joined to *three*. The second criterion thus reveals not only the inequivalence of the $Ta_6Cl_{15}$ and $K_2Zr_6Cl_{15}B$ structures but also their inequivalence to the interpenetrating networks in $Nb_6F_{15}$. The fifth structure type, $K_3Zr_6Cl_{15}Be$, has already been described as related to the $K_2Zr_6Cl_{15}B$ structure through rotations without bond breakage.

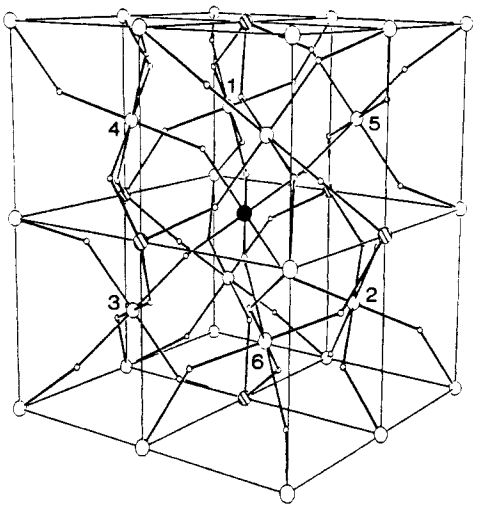


**Figure 12.** Schematic representation of the three-dimensional cluster connectivity in the $Ta_6Cl_{15}$ structure. Large and small spheres represent $M_6Cl^i_{12}$ clusters and $Cl^{a-a}$ atoms, respectively. The open spheres are first-bonding-sphere clusters about the centered black sphere. Cross-hatched spheres are involved in indirectly coupling the FBS clusters.

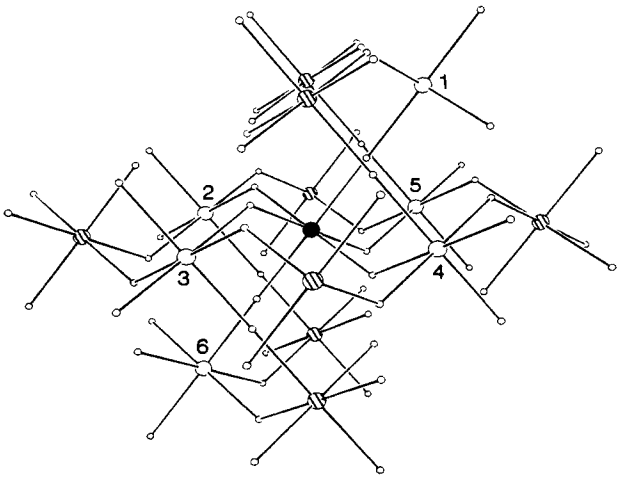


**Figure 13.** Schematic representation of the cluster connectivity in $K_2Zr_6Cl_{15}B$. Large spheres represent $Zr_6Cl^i_{12}B$ clusters while small spheres are bridging $Cl^{a-a}$ atoms. Open ellipsoids are first-bonding-sphere clusters about the solid central cluster. Cross-hatched ellipsoids indirectly connect FBS clusters.

These results clearly illustrate the inadequacy of both a simple $[M_6X^i_{12}]X^{a-a}_{6/2}$ structural description and the view with all $M_6X_{15}$ compounds are simply another folding of the same three-dimensional cluster net around an array of cations. The findings also serve to illuminate the richness and elegance of the structural chemistry of the $M_6X_{15}$ compounds.

**Acknowledgment.** We are indebted to Professor R. A. Jacobson for the continued provision of diffraction and computing facilities. This research was supported by the National Science Foundation, Solid-State Chemistry, via Grant DMR-8318616 and was carried out in facilities of the Ames Laboratory, DOE. R.P.Z. was also the holder of Departmental Proctor and Gamble and Gilman Fellowships.

**Registry No.** $K_2Zr_6Cl_{15}B$, 96929-24-7; $K_3Zr_6Cl_{15}Be$, 112372-99-3; $ZrCl_4$, 10026-11-6; KCl, 7447-40-7; Zr, 7440-67-7; B, 7440-42-8; Be, 7440-41-7.

**Supplementary Material Available:** Tables of anisotropic thermal parameters for $K_2Zr_6Cl_{15}B$ and $K_3Zr_6Cl_{15}Be$ (2 pages); listings of the observed and calculated structure factor data (13 pages). Ordering information is given on any current masthead page.